Strength, elasticity, and equation of state of the nanocrystalline cubic silicon nitride γ-Si_3N_4 to 68 GPa

Boris Kiefer*
Physics Department, New Mexico State University, Las Cruces, New Mexico 88003, USA

Sean R. Shieh
Department of Earth Sciences, National Cheng Kung University, Taiwan

Thomas S. Duffy
Geosciences Department, Princeton University, Princeton, New Jersey 08544, USA

Toshimori Sekine
National Institute of Research in Inorganic Materials (NIRIM), 1-1 Namiki, Tsukuba, Ibaraki 305-0044, Japan
(Received 21 February 2005; revised manuscript received 5 May 2005; published 1 July 2005)

Lattice strains in nanocrystalline cubic silicon nitride were measured using an energy-dispersive x-ray diffraction technique under nonhydrostatic stress conditions up to a confining pressure of 68 GPa. The high-pressure elastic properties of γ-Si_3N_4 were also investigated theoretically using density-functional theory. The differential stress t between 30 and 68 GPa increases from 7 to 23 GPa and can be described beyond 40 GPa as $t=7(4)+0.24(7)P$ where P is the pressure in GPa. The differential stress supported by γ-Si_3N_4 increases with pressure from 3.5% of the shear modulus at 21 GPa to 7.6% at 68 GPa. γ-Si_3N_4 is one of the strongest materials yet studied under extreme compression conditions. The elastic anisotropy of γ-Si_3N_4 is large and only weakly pressure dependent. The elastic anisotropy increases from $A=1.4$ to $A=1.9$ as the parameter α that characterizes stress-strain continuity across grain boundaries is decreased from 1 to 0.5. The high elastic anisotropy compares well with our first-principles calculations that lead to $A=1.92-1.93$ at ambient pressure and $A=1.94-1.95$ at 70 GPa. Using molybdenum as an internal pressure standard, the equation of state depends strongly on ψ, the direction between the diamond cell axis and the normal of the scattering plane. The bulk modulus increases from 224(3) GPa to 460(13) GPa as ψ varies from 0° to 90°. This large variation highlights the need to account properly for deviatoric stresses in nonhydrostatic x-ray diffraction experiments carried out at angles other than the particular angle of $\psi=54.7°$, where deviatoric stress effects on the lattice vanish. At this angle we find a bulk modulus of 339(7) GPa ($K_0'=4$, fixed). This result is in general agreement with our local density approximation calculations, $K_0=321$ GPa, $K_0'=4.0$, and previous shockwave and x-ray diffraction studies. However, our results are significantly lower than the recently reported bulk modulus of $K_0=685(45)$ GPa for nanocrystalline γ-Si_3N_4 below 40 GPa.

DOI: 10.1103/PhysRevB.72.014102 PACS number(s): 61.10.Nz, 62.20.Dc, 62.20.Fe, 62.25.+g

I. INTRODUCTION

A particular challenge in material sciences is the design and synthesis of materials with desired physical properties. It is for this reason that superhard materials have attracted significant interest. Over the past few decades a large number of new compounds with large hardness values have been identified (e.g., Refs. 1 and 2) and this has motivated searches for systematics among physical properties of these materials. Correlation between hardness and elastic properties such as the bulk modulus[1–3] and the shear modulus[1,2] are important for *a priori* materials evaluation. However, ultimately the hardness is determined by the nature of bonding and the crystal structure.[1,2,4] Several general characteristics have emerged from comparative studies as well as the comparison to diamond, the hardest known material: the presence of a high degree of covalent bonding is accompanied by a high bulk modulus[3] and a high shear modulus.[2] A high shear modulus is related to high-bond-bending-force constants and a small number of internal degrees of freedom.[2] Additional insight into high-hardness materials can be obtained by considering phase relations in these systems. Several candidate materials (boron nitride, silicon nitride, germanium nitride) crystallize in a hexagonal structure before transforming into a spinel-type high-pressure polymorph. Spinel may therefore be an important prototype for the design of novel high-hardness materials.[5] The expectation that high pressure may be a promising route to find novel superhard materials is supported further by volume-elasticity systematics that show higher elastic moduli for smaller atomic volumes in an isochemical series of phases.[6]

The Si_3N_4 phases provide an example of the succcess of this strategy. At ambient pressure two phases are known: α-Si_3N_4 (space group $P3_1c$) is the stable structure below 2000 K and the β-Si_3N_4 phase [space group $P6_3$ (Refs. 7 and 8) or $P6_3m$ (Ref. 9)] is stable at higher temperatures. However, at pressures above 15 GPa and 2000 K, γ-Si_3N_4 becomes stable.[10] The same material has also been recovered from shock synthesis experiments[11,12] where the transition from the low-pressure α-Si_3N_4 and β-Si_3N_4 phases to

γ-Si_3N_4 occurred above 20 GPa and reached completion at 63 GPa. γ-Si_3N_4 shows excellent thermal metastability up to at least 1873 K at ambient pressure before it reverts to its low-pressure phases.[13] Electron diffraction shows that γ-Si_3N_4 belongs to spacegroup $Fd\bar{3}m$ (Ref. 10). In this spinel structure, octahedrally and tetrahedrally coordinated Si atoms are fixed by symmetry and the N positions possess a single degree of freedom[10,14] in support of the suggestion that a small number of internal degrees of freedom is a necessary but not sufficient condition for a superhard material.[2] The measured Vickers hardness of γ-Si_3N_4 is between 35 GPa (Ref. 13) and 43 GPa (Refs. 15 and 16) and confirms that this material qualifies as a potentially superhard solid.

The equation of state of γ-Si_3N_4 has been determined from static diamond-anvil-cell (DAC) studies with reported bulk moduli of 290(5) GPa (Ref. 16) and 308(5) GPa (Ref. 17). These bulk moduli are also consistent with that derived from the shock Hugoniot equation of state, 300(10) GPa (Ref. 11). However, the bulk modulus of nanocrystalline γ-Si_3N_4 (grain size between 10 and 50 nm) has been determined to be 685 GPa below a pressure of 40 GPa and 415 GPa above this pressure,[18] significantly higher than in previous experiments. It was proposed in the same study that nanocrystalline γ-Si_3N_4 shows substantial grain size hardening below 40 GPa. (A general trend of increased flow stress with decreasing grain size has been established for simple metals.[19,20] For oxides, the grain size dependence of the equation of state is not clear: bulk moduli of MgO (Ref. 21) and CuO (Ref. 22) are independent of grain size while α-Al_2O_3 shows a decreasing bulk modulus with decreasing grain size.[23])

There are conflicting reports on the shear modulus of γ-Si_3N_4. From nanoindentation measurements, the shear modulus of γ-Si_3N_4 has been indirectly inferred to be 148(16) GPa at ambient conditions.[16] In contrast theoretical studies using density-functional theory predict a shear modulus of 258–282 GPa at ambient pressure[17,24] and theory also predicts an ideal tensile stength of γ-Si_3N_4 of 50 GPa (Ref. 24).

In this study, we examine nanocrystalline γ-Si_3N_4 under nonhydrostatic loading in a diamond anvil cell using x-ray diffraction in a radial geometry. Such experiments measure the variation of the lattice strain with respect to the stress orientation by rotating the DAC for a fixed x-ray scattering geometry.[25–27] From the analysis of these strains[25,28,29] we can investigate directly the effect of nonhydrostatic stress on the equation of state and obtain the ratio of differential stress to shear modulus. However, the determination of the differential stress itself requires the shear modulus. We use first-principles calculations to determine the complete elastic constant tensor of γ-Si_3N_4 up to 70 GPa.

II. METHOD

A. Experimental method

The starting material was shock synthesized γ-Si_3N_4 (Ref. 30). X-ray and electron diffraction[30] confirmed that the recovered sample was γ-Si_3N_4 with residual traces of β-Si_3N_4. The grain size of the powder was determined from TEM to be in the range of 10–50 nm (Ref. 30).

The nanocrystalline sample was loaded into a $\approx$70-μm hole in a Be gasket that was preindented to 20–30 μm thickness. A small Mo foil was placed on one of the culets as pressure marker and as a reference for the x-ray position.[26] A DAC was used to compress the sample nonhydrostatically. Radial x-ray diffraction experiments[27,31] were performed at the X17C beamline of the National Synchrotron Light Source. The incident x-ray beam was focused by a pair of Kirkpatrick-Baez mirrors to approximately 10×15 μm^2 and directed through the Be gasket and the sample. After allowing time for stress relaxation at each compression step (typically less than 2 h) energy-dispersive x-ray diffraction patterns were collected for 15–45 min each at different relative orientations of the DAC axis and the x-ray scattering plane. The hydrostatic pressure at each loading step was determined from the measured lattice constants of Mo at 54.7° and the equation of state of Mo (Ref. 32).

d spacings were obtained by fitting background subtracted Gaussian-Lorentizan line shapes to the spectra. For γ-Si_3N_4 the (220), (311), (400), and (440) lines were used in the analysis (Fig. 2, below). For Mo, the lattice parameter was determined from the (110) diffraction line only. All other Mo peaks had either very low intensities or overlapped with γ-Si_3N_4 diffraction lines.

Lattice strain theory[28,29] describes the variation of lattice strain as a function of stress in a cylindrical geometry. The stress state is characterized by two principal stresses: σ_3 in the axial direction and σ_1 in the radial direction. The hydrostatic stress component is the trace of the stress tensor, $\sigma_P=(\sigma_1+2\sigma_3)/3$, and the deviatoric stress is $t=\sigma_1-\sigma_3\leqslant\sigma_y=2\tau$, where σ_y is the yield strength and τ is the shear strength. The average strain for a particular (*hkl*) diffraction plane is calculated by averaging the strains of all crystallites that contribute to the diffraction peak under consideration.[29] Assuming a random distribution of grain orientations leads to the following set of equations:[25,28,29]

$$a_m(hkl) = a_P[1 + (1 - 3\cos^2\psi)Q(hkl)], \tag{1}$$

where ψ is the angle between the DAC axis and the diffraction plane normal (Fig. 1). a_P is the lattice constant that would result from the application of a hydrostatic pressure, a state that is reached at $\psi=54.7°$ for which the nonhydrostatic stress disappears [Eq. (1)]. $Q(hkl)$ is given by

$$Q(hkl) = \frac{t}{3}\left[\frac{\alpha}{2G_R(hkl)} + \frac{1-\alpha}{2G_V}\right], \tag{2}$$

where t is the differential stress, G_R is the aggregate shear modulus under isostress conditions across grain boundaries, and G_V is the Voigt bound that applies under isostrain conditions and is independent of the grain orientation. α is a parameter that specifies the degree of stress and strain continuity across grain boundaries. For a cubic system, G_R is given by

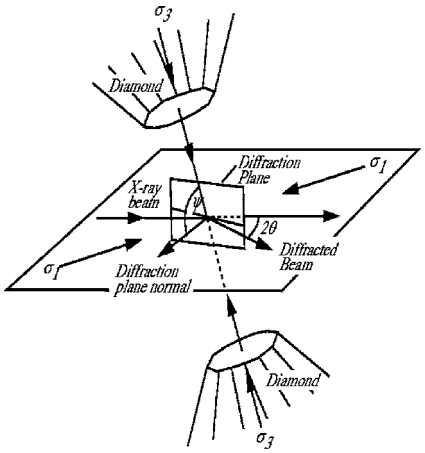

FIG. 1. Experimental geometry of the radial diffraction experiment. The diffraction angle is 2θ, and ψ is the angle between the diffraction plane normal and the diamond anvil cell axis (σ_3).

$$\frac{1}{2G_R(hkl)} = S_{11} - S_{12} - 3S\Gamma, \tag{3}$$

where S, a measure of the elastic anisotropy, has the following form:

$$S = S_{11} - S_{12} - \frac{S_{44}}{2} \tag{4}$$

and

$$\Gamma = \frac{h^2k^2 + h^2l^2 + k^2l^2}{(h^2 + k^2 + l^2)}, \tag{5}$$

$$\frac{1}{2G_V} = \frac{5}{2}\frac{(S_{11} - S_{12})S_{44}}{3(S_{11} - S_{12}) + S_{44}}, \tag{6}$$

where S_{ij} are the single-crystal elastic compliances. It is therefore expected that the lattice parameter for each diffraction plane (hkl) varies linearly with $1-3\cos^2\psi$ [Eq. (1)]. The intercept a_P is the lattice constant at hydrostatic stress conditions and the slope m_1 is related to $Q(hkl)$: $m_1 = a_P Q(hkl)$. The predicted linearity from Eqs. (2) and (3) between $Q(hkl)$ and $\Gamma(hkl)$ implies that the average differential stress can be obtained by averaging $Q(hkl)$. Assuming $\alpha=1$, it follows that

$$t = 6G_R\langle Q(hkl)\rangle, \tag{7}$$

where G_R is the isotropic Reuss shear modulus. More general expressions that hold for any value of α have been given elsewhere.[25] In the same limiting case for α, the intercept (m_0) and slope (m_1) of $Q(hkl)$ vs 3Γ is given as

$$m_0 = \frac{t}{3}[S_{11} - S_{12}] \tag{8}$$

and

$$m_1 = -\frac{t}{3}[S_{11} - S_{12} - S_{44}/2]. \tag{9}$$

For the Zener elastic anisotropy A, the ratio of the shear moduli in the (100) and (110) planes in the [001] direction, it follows that[27]

$$A = \frac{1}{1 + m_0/m_1}, \tag{10}$$

$$A = \frac{2C_{44}}{C_{11} - C_{12}} = 1 + \frac{2S_{12}}{S_{44}}. \tag{11}$$

Lattice strain theory shows that the measurement of lattice parameters under nonhydrostatic stress conditions can give access to a variety of material parameters. At the angle of 54.7°, the macroscopic nonhydrostatic stress is predicted to vanish and a hydrostatic equation of state can be determined. The elastic anisotropy (A) follows from the intercept and the slope of the linear relationship between $Q(hkl)$ and 3Γ [Eq. (10)]. The ratio between differential stress (t) and shear modulus (G_R) can be determined directly from Eq. (7). Once the uniaxial stress component is known, it is possible to determine the individual elastic stiffnesses.[25]

B. Computational method

Our computational method is based on density-functional theory (DFT). The Hamiltonian for the electronic structure calculations preserves the symmetry while allowing the full relaxation of all internal degrees of freedom.[33] The computations were performed with the software package VASP.[34–36] Two approximations are made in the treatment of the many-electron problem: the electrons were described by ultrasoft pseudopotentials[37] and the exchange-correlation potential was described in the local density approximation[38] (LDA). We also performed calculations using the generalized gradient approximation[39] (GGA). Moving the atoms according to the calculated forces allows for an efficient minimization of the total energy. Tests of the computational parameters showed that converged results of the Kohn-Sham equations can be obtained with a plane-wave energy cutoff of 600 eV and a $4\times4\times4$ Monkhorst-Pack[40] grid. The total energies and stresses were converged to within 0.14 and 0.45 meV/atom and 0.02 and 0.04 GPa, for the LDA and GGA respectively. These computational parameters are similiar to the parameters in previous studies of γ-Si_3N_4 at zero pressure.[24,41,42]

γ-Si_3N_4 crystallizes in the space group $Fd\bar{3}m$, with 56 (14) atoms in the conventional (primitive) unit cell.[10] All Si positions in γ-Si_3N_4 are fixed by symmetry in the tetrahedral $8a$ site $(1/8,1/8,1/8)$ and the octaheral $16d$ site $(1/2,1/2,1/2)$. Only the N positions in the $32e$ site (x,x,x) have a single degree of freedom.[10] The three independent elastic stiffnesses of cubic γ-Si_3N_4 were determined in two steps: First, the structure was relaxed into its ground state at a given volume and the pressure was obtained from the trace of the stress tensor. Second, the three independent elastic constants C_{11}, C_{12}, and C_{44} of γ-Si_3N_4 were determined by

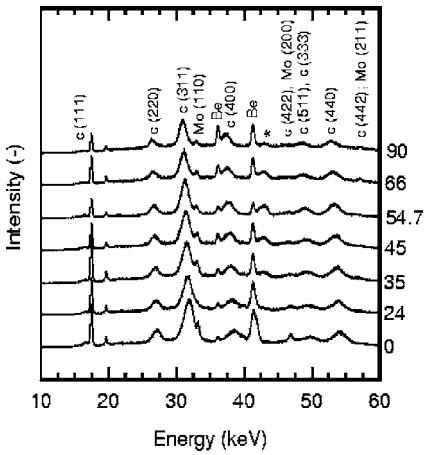

FIG. 2. X-ray diffraction patterns at a pressure of $P=32.7$ GPa. The angles between the DAC axis and the diffraction plane normal are indicated on the right. The diffraction lines, indicated as c, Be, and Mo, belong to γ-Si_3N_4, Be, and Mo, respectively. The two peaks near 20 keV are Mo fluoresence peaks. The $*$ symbol signifies an unidentified peak.

applying small positive and negative strains of magnitude 1% to the relaxed ground-state structure (strain 1: $\epsilon_{11}\neq 0$ all other $\epsilon_{ij}=0$; strain 2: $\epsilon_{44}=\epsilon_{55}=\epsilon_{66}\neq 0$ and all others zero). All internal degrees of freedom were rerelaxed in the strained unit cell to account for the coupling between lattice vibrations and strain. This method has previously been applied successfully to determine elastic properties of insulators.[43,44]

III. RESULTS AND DISCUSSION

Radial x-ray diffraction spectra of γ-Si_3N_4 were collected up to an equivalent hydrostatic pressure of 68 GPa. As expected, the sample peaks shift to lower energies (larger lattice parameter) as ψ increases (Fig. 2). The observed x-ray diffraction lines belong either to γ-Si_3N_4, Mo, or the gasket with the exception of the weak line at an energy of $E=42$ keV (Fig. 2) whose origin is unknown. The total shift in x-ray diffraction lines between the minimum strain (90°) and the maximum strain (0°) orientation is $\approx$0.7 keV (Fig. 2). The Mo foil that is used as a pressure marker also serves as a reference for the DAC axis when the DAC is rotated. However, these two functions of Mo define opposing requirements on the size of the Mo foil: On the one hand, a larger foil allows for rapid sample positioning and stronger diffraction peaks. On the other hand, the theory applies strictly only on the DAC axis[28,29] in favor of smaller Mo foils. To examine the stress distribution, we measured transects across the sample at 0° and 90° (Fig. 3). The pressure in this case was calculated assuming that the measured lattice strain at 0° and 90° corresponds to hydrostatic strain. Both transects show a broad plateau with a diameter of $\approx$50 μm. The static equilibrium equations for deformable media require $\partial\sigma_{rr}/\partial r=0$ on the symmetry axis of the cylinder in order to obtain bound stresses.[45] However, the spatial extent of the plateau is less clear and may depend on the material considered as well as the detailed sample-diamond-gasket geometry.[45] The large

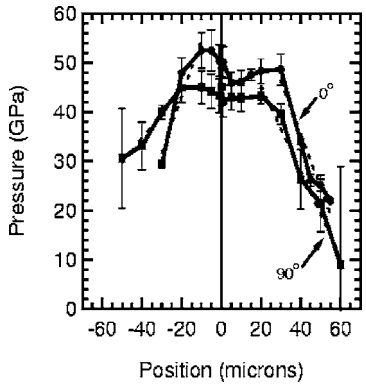

FIG. 3. Apparent pressure gradient across the sample recorded at $\psi=0°$ and 90° for a quasihydrostatic pressure ($\psi=54.7°$) at the sample center of 46.5(0.9) GPa. ψ values (0°, 90°) are shown on the plot. Solid lines are guides to the eye. The dashed lines are linear fits of the pressure gradient.

extent of the observed plateau indicates that lattice strain is rather insensitive to the exact positioning of the x-ray beam, at least in the case of γ-Si_3N_4.

For all diffraction lines, the lattice constants show a linear relationship with $(1-3\cos^2\psi)$ as expected from lattice strain theory[28,29] [Eq. (1) and Fig. 4]. For a cubic material such as γ-Si_3N_4, the equation of state can be determined from each x-ray diffraction line at 54.7°, where the effect of macroscopic nonhydrostatic strain vanishes although microstresses due to the variation in the local stress field are still present.[25] The average volume at a given angle was determined as the arithmetic average of all observed γ-Si_3N_4 diffraction lines. The pressure was determined at 54.7° from the Mo (110) line. It has previously been observed that the Mo (110) diffraction line systematically overestimates the lattice parameter of $\approx$0.1% as compared to other observed Mo diffraction lines.[27] This suggests that the Mo pressure marker may underestimate the pressure by $\Delta P=K\Delta V/V$ where K is the bulk modulus at pressure and $\Delta V/V$ is the volume change. Using the Mo shock-wave equation of state[32] with $K\approx 411$ GPa at 70 GPa and $\Delta V/V\approx 0.3$ results in a deviation of $\approx$1.5 GPa

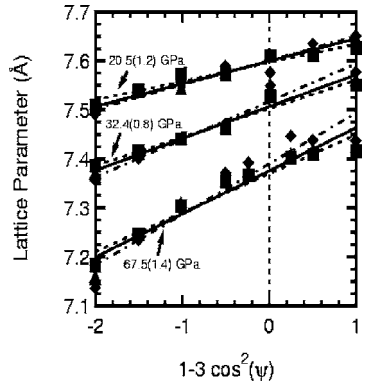

FIG. 4. Dependence of lattice spacing on $1-3\cos^2\psi$ at selected pressures for γ-Si_3N_4. Squares: (220). Triangles: (311). Diamond: (400). The lines are least-squares fits to the data: dashed line, solid line, and dot-dashed line, for (220), (311), and (400), respectively. Errors are less than the size of the symbols.

TABLE I. Equation of state of γ-Si_3N_4. The 300 K theoretical values were calculated using a Mie-Grueneisen equation of state, with $\gamma_0=1.2$ and $q=\partial \ln \gamma/\partial V=1$ (Ref. 11). Zero-point motion and thermal effects were calculated within a Debye model using the acoustic Debye temperature.

Ref.	V_0 (Å^3)	K_0 (GPa)	K_0' (-)
	Experiment		
This study $\psi=54.7°$	464.1(4)	339(7)	4 (fixed)
This study $\psi=0°$	464.1(4)	224(3)	4 (fixed)
This study $\psi=90°$	464.1(4)	460(13)	4 (fixed)
Ref. 17	464.2(1.7)	308(5)	4.0(2)
Ref. 11	—	300(10)	3(1)
Ref. 18	461.7(6)	685(45)	4 (fixed)
Ref. 16	463.1(1.1)	290(5)	4.9(6)
	Theory		
This study: LDA, 0 K	452.6	321.5	4.00
LDA, 300 K	457.4	309.9	4.02
This study: GGA, 0 K	471.9	287.7	4.01
GGA, 300 K	477.2	276.9	4.02
Ref. 47 (HF-aiPI)	408.4	407	3.33
Ref. 41 (LDA)	456.0	308	3.9
Ref. 41 (GGA)	473.2	284	3.9
Ref. 42 (PAW-LDA)	455.8	321	–
Ref. 42 (PAW-GGA)	472.5	285	–
Ref. 48 (quantum chemical)	483.0	335	–

at the highest quasihydrostatic pressure in our study.

At ambient pressure we obtain a volume of $V_0=464.1(4)$ Å^3 from a powder x-ray diffraction pattern obtained before compression, consistent with $V_0=464.4(1.9)$ Å^3, the volume of the shock-recovered sample[30] and previous DAC experiments.[16,41] The equation-of-state parameters at 0°, 54.7°, and 90° were obtained from a fit to a second-order Birch-Murnahan equation of state[46] with $V_0=464.1$ Å^3 and $K_0'=4$ fixed. The resulting bulk moduli are 224(3) GPs, 339(7) GPa, and 460(13) GPa for $\psi=0°$, $\psi=54.7°$, and $\psi=90°$, respectively (Table I and Fig. 5).

The equation of state as obtained for the quasihydrostatic stress state ($\psi=54.7°$) is in agreement with previous hydrostatic equation of state measurements[17] [Fig. 5(a)]. It is noted that the quasihydrostatic bulk modulus in the present study is ≈12% (for $K_0'=4$) higher than DAC experiments on γ-Si_3N_4 in a N_2 pressure medium.[17] This agreement is reasonable in view of the limited number of data points in the present study. Our measured volumes generally overlap with those of Ref. 17 in the common pressure range although our data tend towards slightly larger volumes. Nevertheless, a slighlty high bulk modulus has been observed in radial diffraction experiments on Au/Re samples[26] and Mo/Au samples.[27] This difference can be caused by a variety of factors such as nonvanishing microstresses or pressure differences between sample and pressure marker.[26]

The results of the static first-principles calculations of the equation of state are in good agreement with previous calculations[17,24,42] [Fig. 5(a) and Table I]. For a more direct comparison between theory and experiment, the pressure due to zero-point motion and 300-K temperature difference was calculated within a Debye model. We find that zero-point motion contributes ≈80% to the correction while ≈20% are due to the 300-K temperature difference between theory and experiment. Accouting for vibrational effects and zero-point motion improves the agreement between the LDA calculations and experiment [Fig. 5(a) and Table I]: the zero-pressure volume is underestimated by less than 1.5% and the bulk modulus is within the experimental error. For the GGA, the static zero-pressure volume was already higher than experiment and therefore the deviations increase as vibrational effects and zero-point motion are included. The remaining discrepancy is attributed to the exchange correlation potential and the pseudopotential. It is expected that the bulk modulus is further reduced as the zero-pressure volume is increased to match the experimentally observed ambient-pressure volume. Therefore the calculated LDA value may constitute an upper bound for the bulk modulus.

The direct comparison of the 0° and 90° equation of state [Fig. 5(b) and Table I] shows that the bulk modulus varies by more than a factor 2 for data collected at 0° and 90°. This

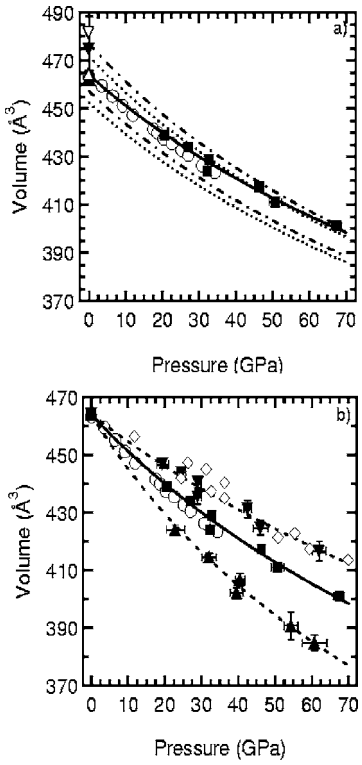

FIG. 5. Equation of state of γ-Si_3N_4. (a) Radial diffraction at 54.7°: Solid squares: radial diffraction. Solid line: second-order Birch-Murnahan equation of state. Open circles: Ref. 41. Solid down triangle: Ref. 10. Solid up triangle: Ref. 14. Open up triangle: Ref. 30. Open down triangle: Ref. 8. Theory: lower (upper) dashed line, LDA (GGA) static calculations, this study; lower (upper) dot-dashed line, LDA (GGA) 300 K isotherm. (b) Dependence of the equation of state on the orientation of DAC stress axis and the normal of the diffraction planes. This study: $\psi=0°$, triangles up; 54.7°, solid squares; and 90°, open triangles down. Open diamonds: Ref. 18. Open circles: Ref. 41.

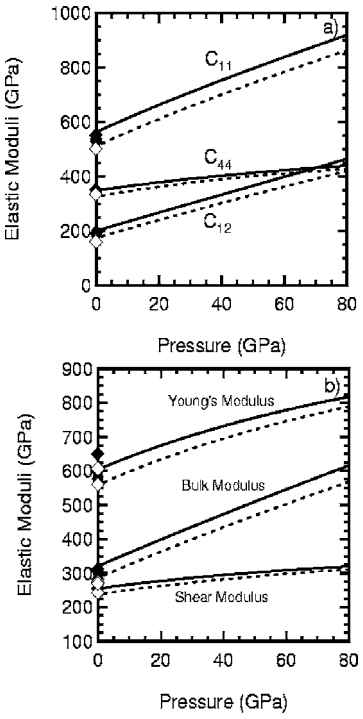

FIG. 6. Elasticity of γ-Si_3N_4. (a) Second-order elastic moduli of γ-Si_3N_4 as a function of pressure. LDA: solid lines. GGA: dashed lines. Previous theoretical studies: solid circles from Ref. 41; solid diamonds, open diamonds, LDA and GGA, respectively, from Ref. 24. (b) Isotropic elastic moduli for γ-Si_3N_4. Symbols are the same as in panel (a).

suggests that the very high bulk modulus of 685(45) GPa reported recently for nanocrystalline γ-Si_3N_4 (Ref. 18) is likely due to nonhydrostatic stress in the experiment. The experiments were done without a pressure medium, close to a 90° scattering geometry. The sample used in Ref. 18 was also shock synthesized and of similiar grain size as that in the present study. Lattice strain theory together with theoretically calculated elastic constants (see below) allows us to predict the expected order of the lattice spacing for this geometry due to nonhydrostatic stress. For γ-Si_3N_4 the predicted order of the lattice parameter is $a(111)<a(220)<a(311)<a(511)<a(400)$. The order is generally consistent with the observed order in Ref. 18. Indeed we find that their equation of state follows closely our 90° nonhydrostatic equation of state [Fig. 5(b)]. Similiar conclusions likely apply to the very large bulk modulus values reported for nanocrystalline γ-Ge_3N_4 as well.[49] The effect of grain size on the bulk modulus of oxides and nitrides is generally unclear as discussed above. The consistency of the experimental and theoretical bulk moduli suggests an upper bound of $K_0=310-320$ GPa for γ-Si_3N_4, and it may be speculated that the remaining 12% difference is the maximum amount that can be attributed to grain size effects.

We calculated the complete elastic constant tensor for γ-Si_3N_4 up to 70 GPa from first principles. At zero pressure, our calculations are in good agreement with previous theoretical studies [Fig. 6(a) and Table II]. The pressure dependence of the elastic constants has been described within the Eulerian finite-strain formalism.[50] We observe that the GGA elastic constants are systematically lower than the LDA elastic constants, consistent with the larger zero-pressure volume of the GGA calculation (Table I). The elastic constants as obtained from the LDA and GGA calculations follow parallel trends with an offset in pressure of $\approx$13 GPa roughly similiar to the offset of the equation of state [Fig. 5(a)]. Therefore LDA and GGA are mutually consistent if they are compared at constant volume rather than constant pressure. At low pressures we observe that $C_{11} \gg C_{44} \gg C_{12}$ with $C_{44}/C_{12} \approx 1.75$. It is instructive to compare these values with other materials with spinel-type structure such as γ-Mg_2SiO_4 and $MgAl_2O_4$. These oxides also show the same order of the elastic stiffnesses[51] but $C_{44}/C_{12} \approx 1-1.2$ is much lower than for γ-Si_3N_4. The isotructural γ-Ge_3N_4 is intermediate with $C_{44}/C_{12} \approx 1.4$ (Ref. 17). This observation is consistent with increased covalent bonding in γ-Si_3N_4 as compared with γ-Ge_3N_4. The effect of pressure is to reduce the C_{44}/C_{12} ratio such that it is close to 1 at the highest pressures [Fig. 6(a)]. Nevertheless, the Cauchy violation ($C_{12}-C_{44}-2P$, where P is the hydrostatic pressure) of γ-Si_3N_4 remains large and changes only little with pressure, from −149 GPa at zero pressure to −140 GPa at 70 GPa. This indicates that a high C_{44}/C_{12} ratio, favorable for a high shear modulus,[2] can be deceiving if used as a proxy for bond character in materials.

Lattice strain theory allows determination of the Zener elastic ansiotropy ratio from the linear relationship between $Q(hkl)$ and $3\Gamma(hkl)$ [Fig. 7 and Eqs. (8)–(10)].

We find that γ-Si_3N_4 has a large elastic anisotropy A of 1.39(22) at 20.5(1.2) GPa that increases only slightly to $A=1.44(2)$ at 67.5(1.4) GPa. A large and weakly-pressure-dependent elastic anisotropy factor is consistent with our first-principles calculations. The elastic anisotropy ratio for the LDA (GGA) changes from $A=1.93(1.94)$ at ambient pressure to $A=1.92(1.93)$ at 68 GPa. The calculated elastic

TABLE II. Elastic constants and aggregate elastic properties and pressure derivatives for γ-Si_3N_4 as obtained from theory. Elastic moduli in GPa, pressure derivatives are given in parentheses, where available.

C_{11}	C_{12}	C_{44}	K_0	G_R	G_V	Reference
562.9 (5.22)	200.3 (3.38)	348.8 (1.69)	321.2 (3.99)	254.7 (1.3)	281.8 (1.4)	This study: LDA (static)
510.9 (5.24)	173.6 (3.42)	325.8 (2.11)	286.0 (4.03)	237.4 (1.4)	262.9 (1.6)	This study: GGA (static)
550.6	191.0	349.4	310.9	253.7	281.6	Ref. 24: LDA
499.6	159.0	333.6	272.5	241.1	268.3	Ref. 24: GGA
532.6	191.2	341.0	305.0	243.7	258.3	Ref. 41: LDA

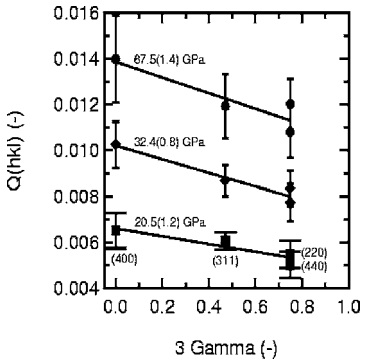

FIG. 7. $Q(hkl)$ versus 3Γ for γ-Si_3N_4 at selected pressures. Pressures are obtained from the quasihydrostatic ($\psi=54.7°$) equation of state. The errors were propagated from deviations of the $a(hkl)$ vs $1-3\cos^2\psi$ data.

constants at pressure provide an explanation for this weak pressure dependence of A: The pressure derivatives of $\partial(C_{11}-C_{12})/\partial P \approx 1.8$ at zero pressure almost balance the pressure derivative of C_{44} (Table II). The differences of 38% between experiment and theory may be explained by the assumption of $\alpha=1$ in the analysis. While theory and experiment are qualitatively in agreement with regard to the elastic anisotropy, quantitative differences could be related to the stress-strain continuity parameter α. If α is reduced from 1 to 0.5, the elastic anisotropy factor increases from 1.4 to 1.9. Another possibility is that the lattice strain is affected by plastic anisotropy and therefore is not a measure of pure elastic anisotropy.[52]

The elastic constant tensors of many spinel-structured oxides have been measured, and they consistently show elastic anisotropy greater than 1 (Ref. 51). Some spinels are highly anisotropic ($A=2.5$, $MgAl_2O_4$) but others display modest or weak anisotropy ($A=1.2$, γ-$MgSi_2O_4$). Lattice strain measurements in the diamond anvil cell have previously been reported on two spinels: dry and hydrous ringwoodites (γ-$MgSi_2O_4$) (Refs. 53 and 54). A surprising feature of these results was that the anisotropy determined by lattice strain theory was less than 1, which is inconsistent with previous experimental data[55,56] and theoretical predictions[44] for ringwoodite. (We note that the anisotropies in Ref. 53 are incorrectly plotted. The correct values are in Ref. 54.) Using a model of plastic anisotropy, it has been suggested that this discrepancy is due to a dominant role of strength, rather than elastic, anisotropy.[52] For another silicate, $CaSiO_3$ in the perovskite structure, although the elastic anisotropy from lattice strain is consistent with theoretical predictions, some evidence for strength anisotropy has been reported.[57] On balance, our results indicate a significant difference between the theoretically and experimentally determined elastic anisotropy of γ-Si_3N_4, further emphasizing caution in the interpretation of elasticity from lattice strain results under the assumption of elastic behavior in the Reuss limit. In comparison with other spinels, however, the lattice strain results are qualitatively consistent with density-functional theory in that the elastic anisotropy is significantly larger than 1 and relatively constant with pressure.

The aggregate elastic properties of γ-Si_3N_4 calculated from theory are shown in Fig. 6(b). From third-order Eulerian finite-strain fits[50] of the elastic stiffnesses, we obtained a pressure derivative of the shear modulus of 1.3 and 1.4 for the LDA and GGA (Table II), respectively. These pressure derivatives are consistent with values found for other hard materials, typically in the range of 1–1.5 (Ref. 51). The calculated LDA (GGA) Poisson's ratio varies from 0.161 (0.148) to 0.249 (0.237) as pressure is increased from 0 to 68 GPa.

The determination of the yield strength from lattice strain theory requires an elastic model. In our study we take this input from our LDA calculations. Lattice strain theory couples elastic and plastic deformation through[26–28] $\langle t\rangle = 6G\langle Q(hkl)\rangle f(A,\alpha,(hkl))$ where $\langle t\rangle$ is the differential stress and $\langle Q(hkl)\rangle = \Sigma Q(hkl)/n$ is the average lattice strain as experienced by the n observed x-ray diffraction planes. We find in agreement with previous studies[25–27] that the factor $f(A,\alpha,(hkl))=1$ to within $\approx 5\%$. Furthermore, this factor depends only weakly on α and A. Therefore we assumed $f(A,\alpha,(hkl))=1$ for this analysis. With these assumptions the ratio of differential stress (t) and shear modulus (G), $t/G = 6\langle Q_{hkl}\rangle$, is independent of the elastic model and can be obtained directly from the measured peak shifts. The quantity t/G changes from 0.0347(17) at 20.5(1.2) GPa to 0.0763(38) at 67.5(1.4) GPa [Fig. 8(a)]. Boron suboxide is another potentially superhard solid with bulk and shear moduli of 230 GPa and 206 GPa at ambient pressure, respectively.[58] It exhibits t/G values that are about 30% larger than those found here for γ-Si_3N_4.

Figure 8(a) shows that t/G values are generally large for high-hardness materials as compared to other classes of materials such as metals and silicates. These observations support previous suggestions that strong covalent (directional) bonds are necessary but may not be suffucient for the formation of superhard materials. γ-Si_3N_4 is a high-hardness material not only due to its high aggregate shear modulus [Fig. 6(b)], but also for its intrinsic stength. High t/G values in spinel-type structures support the the suggestion[5] that this structure type could be suited as a structural template for the design of superhard materials.

We combined the calculated elastic constant tensor with the radial diffraction measurements to determine the absolute values of the differential stress. Linear regression of the differential stress above 40 GPa gives $t=7(4)+0.24(7)P$. Alternatively the differential stress can be calculated from the pressure gradient across the sample (Fig. 3) from the relationship $t=h\partial P/\partial r$, where h is the thickness of the sample under compression and P is the pressure as obtained from the 0° or 90° equation of state.[45] Assuming a sample thickness of 20 μm, we obtain values for t between 10(1) GPa and 23(8) GPa with an average of 18(4) GPa at a pressure of 46.5 GPa. This value is consistent with the uniaxial stress obtained from the lattice strain measurements.

The differential stress of γ-Si_3N_4 is very large [Fig. 8(b)] due to its large t/G and shear modulus values. The differential stress corresponds to the compressive yield strength for a sample that has exceeded its yield point or is a lower bound on the strength if yield has not yet been reached. The slope

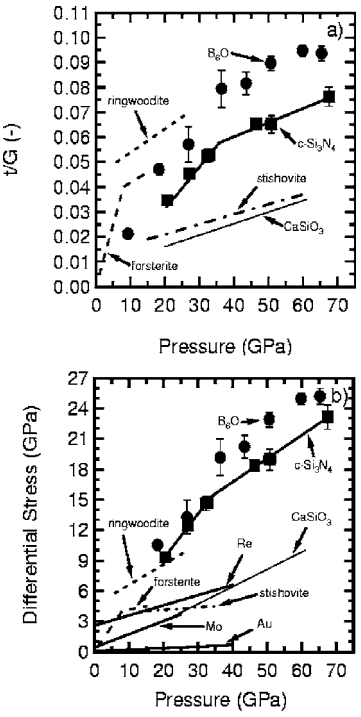

FIG. 8. (a) Ratio of differential stress to Reuss shear modulus as a function of pressure. Solid squares: this study, radial diffraction. Solid line: linear fits to present data. Short-dashed line: Ringwoodite (Ref. 53). Long-dashed line: Forsterite (Ref. 59). Dot-dashed line: SiO_2 stishovite (Ref. 31). Thin solid line: $CaSiO_3$ perovskite (Ref. 57). Solid circles: B_6O (Ref. 60). (b) Differential stress. Re, Mo, and Au (Refs. 26 and 27); other symbols and references are the same as in panel (a).

of the t versus pressure relation becomes shallower above 35 GPa [Fig. 8(b)]. This change in slope suggests that the yield point was reached near this pressure. Similar behavior was observed for B_6O (Ref. 60). The differential stress supported by γ-Si_3N_4 is comparable to that found in B_6O, as γ-Si_3N_4 has a larger shear modulus which partially compensates for the higher t/G values found in B_6O. These materials are the strongest yet measured at high pressure in uniaxial diamond-anvil-cell experiments. The stength of polycrystalline materials is also known to increase with decreasing grain size, and grain-size differences need also to be considered in comparing γ-Si_3N_4 (nanocrystalline) and B_6O (microcrystalline). Grain-size effects on high-pressure strength have been documented previously in radial diffraction experiments.[61]

Metals and oxides show smaller values of differential stress [Fig. 8(b)]. Another high-hardness material is SiO_2 stishovite with a Vicker's hardness of 33 GPa (Ref. 62). However, its lower t/G values [Fig. 8(a)] in conjunction with a softening of the shear modulus at pressure also lead to a modest absolute value of the differential stress [Fig. 8(b)].

The strong increase of t/G above the yield point for γ-Si_3N_4 indicates that the strength under compression increases considerably more rapidly than the shear modulus for nanocyrystalline γ-Si_3N_4. This is also true for other classes of materials investigated to date [Fig. 8(b)]. Thus, the yield strength increases more rapidly with compression than predicted by simple scaling models.[63–65]

It has been suggested that once the yield strength is reached the measured lattice strain no longer reflects the elastic anisotropy but is controlled by plastic anisotropy.[52] We therefore analyzed the lattice strains as experienced by individual x-ray diffraction lines for their strength anisotropy by applying the relationship $t(hkl)=6G_R(hkl)Q(hkl)$ to each diffraction line individually. Within the resolution of our data, we could not find evidence for strength anisotropy.

IV. CONCLUSION

The high-pressure behavior of cubic silicon nitride has been investigated experimentally using radial x-ray diffraction techniques in a diamond anvil cell and theoretically using density functional theory (LDA and GGA). The sample studied was shock synthesized and had a grain size of 10–50 nm. Our results provide new constraints on the elasticity, equation of state, and strength of nanocrystalline γ-Si_3N_4 at high pressures. The main conclusions are as follows.

(i) The quasihydrostatic equation of state for γ-Si_3N_4 obtained from nonhydrostatic x-ray diffraction at the appropriate angle between diffraction vector and stress axis yields a bulk modulus of 339(7) GPa (for fixed $K_0'=4$) which is $\approx$12% higher than found from our first-principles calculations and most previous theory and experiments on microcrystalline samples.

(ii) The bulk modulus from both theory and experiment determined here is nevertheless dramatically lower by about a factor of 2 than that found in a previous compression study (Ref. 18) on nanocrystalline γ-Si_3N_4 of similar particle size as this study. A comparison of both averaged volumes and ordering of lattice parameters from individual diffraction lines indicates that the large bulk modulus obtained previously is mainly due to the combined effects of nonhydrostatic stress and sample geometry, not small grain size.

(iii) Based on the above, we conclude that the maximum effect of the nanocrystalline grain size would be to produce a 12% increase in the bulk modulus. However, there are other possible explanations for the differences between K_0 from radial diffraction and theory.

(iv) The elastic constant tensor of γ-Si_3N_4 has been computed up to 68 GPa using density-functional theory. Our ambient pressure results agree well with previous calculations, and we provide the first determinations of the elastic tensor at high pressures. The pressure derivative of the Reuss shear modulus is 1.3 and 1.4 at ambient pressure for the LDA and GGA, respectively. The elastic anistropy $A=2C_{44}/(C_{11}-C_{12})$ is found to be 1.92–1.94 at high pressure, compared with 1.39–1.44 from the lattice strain experiments. There is thus agreement that γ-Si_3N_4 retains strong elastic anisotropy under compression with a Zener anisotropy ratio greater than 1. Differences between theory and experiment could be related to degree of stress-strain continuity (α parameter), plastic anisotropy, and experimental and theoretical uncertainties. We note, however, that no direct evidence for strength anisotropy has been identified.

(v) The differential stress supported by γ-Si_3N_4 increases with pressure from 3.5% of the shear modulus at 20.5(1.2) GPa to 7.6% of G at 67.5(1.4) GPa. Combining these results with theoretical values for the shear modulus, the supported differential stress ranges from 7 GPa at 32.4(0.8) GPa to 23 GPa at 67.5(1.4) GPa. B_6O and γ-Si_3N_4 exhibit similar differential stress values at high pressure and are the strongest materials yet studied under these extreme compression conditions.

ACKNOWLEDGMENTS

We thank J. Hu for experimental assistance and S. Speziale for helpful discussions. This work was supported by the NSF and the Carnegie-DOE Alliance Center (CDAC), through the Department of Energy and Stewardship Science Academic Alliances Program, under Grant DE FC03-03NA00144.

*Author to whom correspondence should be addressed. Electronic address: bkiefer@nmsu.edu

[1] D. M. Teter, MRS Bull. **23**, 22 (1998).
[2] J. Haines, L. M. Léger, and G. Bocquillon, Annu. Rev. Mater. Sci. **31**, 1 (2001).
[3] A. Y. Liu and M. L. Cohen, Science **245**, 841 (1989).
[4] J. M. Recio, R. Franco, A. Martín Pendás, M. A. Blanco, L. Pueyo, and R. Pandey, Phys. Rev. B **63**, 184101 (2001).
[5] J. E. Lowther, J. Am. Ceram. Soc. **85**, 55 (2002).
[6] A. Martín Pendás, A. Costales, M. A. Blanco, J. M. Recio, and V. Luaña, Phys. Rev. B **62**, 13970 (2000).
[7] Y. Bando, Acta Crystallogr., Sect. B: Struct. Sci. **39**, 185 (1983).
[8] W. Y. Ching, L. Ouyang, and J. D. Gale, Phys. Rev. B **61**, 8696 (2000).
[9] M. Billy, J.-C. Labbe, A. Selvaraj, and G. Roult, Mater. Res. Bull. **18**, 921 (1983).
[10] A. Zerr, G. Miehe, G. Serghiou, M. Schwarz, E. Kroke, R. Riedel, H. Fuess, P. Kroll, and R. Boehler, Nature (London) **400**, 340 (1999).
[11] H. He, T. Sekine, T. Kobayashi, H. Hirosaki, and I. Suzuki, Phys. Rev. B **62**, 11412 (2000).
[12] T. Sekine, J. Am. Ceram. Soc. **85**, 113 (2002).
[13] J. Z. Jiang, F. Kragh, D. J. Frost, K. Ståhl, and H. Lindelov, J. Phys.: Condens. Matter **13**, L515 (2001).
[14] J. Z. Jiang, K. Ståhl, R. W. Berg, D. J. Frost, T. J. Zhou, and P. X. Shi, Europhys. Lett. **51**, 62 (2000).
[15] I. Tanaka, F. Oba, T. Sekine, E. Ito, A. Kubo, K. Tatsumi, H. Adachi, and T. Yamamoto, J. Mater. Res. **17**, 731 (2002).
[16] A. Zerr, M. Kempf, M. Schwarz, E. Kroke, M. Goken, and R. Riedel, J. Am. Ceram. Soc. **85**, 86 (2002).
[17] E. Soignard, M. Somayazulu, J. Dong, O. F. Sankey, and P. F. McMillan, J. Phys.: Condens. Matter **13**, 557 (2001).
[18] Z. Wang, Y. Zhao, D. Schiferl, C. S. Zha, R. T. Downs, and T. Sekine, Appl. Phys. Lett. **83**, 3174 (2003).
[19] J. Schiotz and K. W. Jacobsen, Science **301**, 1357 (2003).
[20] Z. Budrovic, H. V. Swygenhoven, P. M. Drelet, S. V. Petegem, and B. Schmitt, Science **304**, 273 (2004).
[21] S. Rekhi, S. K. Saxena, Z. D. Atlas, and J. Hu, Solid State Commun. **117**, 33 (2001).
[22] Z. Wang, V. Pischedda, S. K. Saxena, and P. Lazor, Solid State Commun. **121**, 275 (2002).
[23] B. Chen, D. Penwell, L. R. Benedetti, R. Jeanloz, and M. B. Kruger, Phys. Rev. B **66**, 144101 (2002).
[24] C. Kocer, N. Hirosaki, and S. Ogata, Phys. Rev. B **67**, 035210 (2003).
[25] A. K. Singh, C. Balasingh, H.-K. Mao, R. J. Hemley, and J. Shu, J. Appl. Phys. **83**, 7567 (1998).
[26] T. S. Duffy, G. Shen, D. Heinz, J. Shu, Y. Ma, H.-K. Mao, R. J. Hemley, and A. K. Singh, J. Appl. Phys. **60**, 15063 (1999).
[27] T. S. Duffy, G. Shen, J. Shu, H.-K. Mao, R. J. Hemley, and A. K. Singh, J. Appl. Phys. **86**, 6729 (1999).
[28] A. K. Singh, J. Appl. Phys. **74**, 5920 (1993).
[29] A. K. Singh, J. Appl. Phys. **73**, 4278 (1993).
[30] T. Sekine, H. He, T. Kobayashi, M. Zhang, and F. Xu, Appl. Phys. Lett. **76**, 3706 (2000).
[31] S. R. Shieh, T. S. Duffy, and B. Li, Phys. Rev. Lett. **89**, 255507 (2002).
[32] R. S. Hixon and J. N. Fritz, J. Appl. Phys. **71**, 1721 (1992).
[33] R. M. Wentzcovitch, J. L. Martins, and G. D. Price, Phys. Rev. Lett. **70**, 3947 (1993).
[34] G. Kresse and J. Hafner, Phys. Rev. B **47**, R558 (1993).
[35] G. Kresse and J. Furthmuller, Comput. Mater. Sci. **6**, 15 (1996).
[36] G. Kresse and J. Furthmuller, Phys. Rev. B **54**, 11169 (1996).
[37] D. Vanderbilt, Phys. Rev. B **41**, R7892 (1990).
[38] D. M. Ceperley and B. J. Alder, Phys. Rev. Lett. **45**, 566 (1980).
[39] J. P. Perdew, J. A. Chevary, S. H. Vosko, K. A. Jackson, M. R. Pederson, D. J. Singh, and C. Fiolhais, Phys. Rev. B **46**, 6671 (1992).
[40] H. J. Monkhorst and J. D. Pack, Phys. Rev. B **13**, 5188 (1976).
[41] E. Soignard, M. Somayazulu, H.-K. Mao, J. Dong, O. F. Sankey, and P. F. McMillan, Solid State Commun. **120**, 237 (2001).
[42] C. M. Fang, G. A. de Wijs, H. T. Hintzen, and G. de With, J. Appl. Phys. **93**, 5175 (2003).
[43] B. B. Karki, L. Stixrude, S. J. Clark, M. C. Warren, G. J. Ackland, and J. Crain, Am. Mineral. **82**, 52 (1997).
[44] B. Kiefer, L. Stixrude, and R. M. Wentzcovitch, Geophys. Res. Lett. **24**, 2841 (1997).
[45] C. Meade and R. Jeanloz, J. Geophys. Res. **93**, 3261 (1988).
[46] F. Birch, J. Geophys. Res. **83**, 1257 (1978).
[47] P. Mori-Sánchez, R. Franco, A. M. Pendás, V. Luana, and J. M. Recio, Europhys. Lett. **54**, 760 (2001).
[48] P. Mori-Sánchez, M. Marqués, A. Beltrán, J. Z. Jiang, L. Gerward, and J. M. Recio, Phys. Rev. B **68**, 064115 (2003).
[49] Z. Wang, Y. Zhao, D. Schiferl, J. Qian, R. T. Downs, H.-K. Mao, and T. Sekine, J. Phys. Chem. **107**, 14151 (2003).
[50] G. F. Davies, J. Phys. Chem. Solids **35**, 1513 (1974).
[51] D. G. Isaak, in *Handbook of Elastic Properties of Solids, Liquids, and Gases*, edited by M. Levy, E. Bass, R. R. Stern, and V. Keepens (Academic Press, San Diego, CA, 2001), Vol. III, pp. 325–377.
[52] D. J. Weidner, L. Li, M. Davis, and J. H. Chen, Geophys. Res. Lett. **31**, L06621 (2004).

[53] A. Kavner and T. S. Duffy, Geophys. Res. Lett. **28**, 2691 (2001).
[54] A. Kavner, Earth Planet. Sci. Lett. **214**, 645 (2003).
[55] D. J. Weidner, H. Sawamoto, S. Sasaki, and M. Kumazawa, J. Geophys. Res. **89**, 7852 (1984).
[56] J. M. Jackson, S. V. Sinogeikin, and J. D. Bass, Am. Mineral. **85**, 296 (2000).
[57] S. R. Shieh, T. S. Duffy, and G. Shen, Phys. Earth Planet. Inter. **143–144**, 93 (2004).
[58] D. R. Petrak, R. Ruh, and G. R. Atkins, Am. Ceram. Soc. Bull. **83**, 569 (1974).
[59] T. Uchida, N. Funamori, T. Ohtani, and Y. Yagi (unpublished).
[60] D. He, S. R. Shieh, and T. S. Duffy, Phys. Rev. B **70**, 184121 (2004).
[61] A. K. Singh, H. P. Liermann, and S. K. Saxena, Solid State Commun. **132**, 795 (2004).
[62] V. V. Brazhkin, M. Grimsditch, I. Guedes, N. A. Bendeliani, T. I. Dyuzheva, and L. M. Lityagina, Phys. Usp. **45**, 447 (2002).
[63] J. O. Chua and A. L. Ruoff, J. Appl. Phys. **46**, 4659 (1975).
[64] J. O. Chua, A. L. Ruoff, D. J. Steinberg, S. G. Cochran, and J. Guinan, J. Appl. Phys. **51**, 1498 (1980).
[65] D. J. Steinberg, S. G. Cochran, and M. W. Guinan, J. Appl. Phys. **51**, 1498 (1980).